AIAA JOURNAL
Vol. 40, No. 5, May 2002

Specific Impulse and Other Characteristics of Elementary Propellants for Ablative Laser Propulsion

Andrew V. Pakhomov,* Don A. Gregory,† and Michael S. Thompson‡
University of Alabama in Huntsville, Huntsville, Alabama 35899

This work was performed as a continuation of ablative laser propulsion (ALP) research recently revived by the authors. An ALP-based space vehicle would be driven by high-energy, short-duration (10^{-10} s and less) laser pulses, focused on a solid propellant. Under such irradiation conditions, plasma and laser pulses are temporally separated, and the direct ablation of solid propellant dominates other possible momentum transfer mechanisms. The studies were performed for various elemental targets, ablated at irradiances up to $\sim 3 \times 10^{13}$ W/cm^2 delivered by 100-ps laser pulses at a wavelength of 532 nm. The data, collected predominantly from time-of-flight technique, include ion velocities, number densities, ion density angular distributions, and mass-removal rates. From these data, specific impulses and net momenta exerted on targets by ablation were calculated. For the irradiation conditions used, the highest I_{sp} and lowest mass-removal rates were achieved for low-Z targets, whereas high-Z elements provided higher momenta. The upper limits for I_{sp} derived from ion velocity reached 2×10^4 s with carbon (graphite). Ion energies varied from element to element in the range of $\sim$ 0.4–2.0 keV, with ion fractions of $\sim$ 0.8–3.8% and mass-removal rates in the range of 0.1–3.0 μg per laser pulse. Ion velocities exhibit Maxwellian distributions, whereas ion number densities in the plasma plume were fitted to a cosine function. All studied characteristics indicate that high-I_{sp} ALP must be based on solid low-Z propellants such as a carbon or aluminum.

Introduction

LASER propulsion (LP), perhaps one of the most realistic advanced propulsion concepts, is currently approaching practical realization. From the first formulation of the concept[1] to the flight demonstrations in New Mexico,[2] LP passed through a period of conceptual proofs and is now ready for a broad and intense research and development phase. In a previous paper[3] arguments were presented that showed that the most efficient scheme for LP is ablative laser propulsion (ALP). The analysis was based on the fact that a majority of the different schemes proposed for laser propulsion over the years (see reviews in Refs. 4 and 5 and references therein) had much in common. 1) They employed continuous-wave irradiation (microsecond pulses fall into this category in terms of plasma lifetime) leading to momentum transfer through compression waves in a laser-sustained plasma or overheated gas, and 2) fluids were often proposed as propellants. In contrast to this (see Ref. 3 for detailed discussion), the ALP-based craft is driven by high-energy, short-width (10^{-10} s and less) laser pulses focused on a solid propellant. Under such irradiation conditions direct ablation of propellant dominates the momentum transfer. It was shown in the previous paper[3] that ALP is the optimum technique in terms of energy efficiency, providing better specific impulses and mass-power ratios than any other LP approach. In contrast to other LP schemes, ALP also appears to be strictly material dependent.

The choice of a proper solid propellant for an ALP-driven vehicle is perhaps the only area of concern where a broad range of opportunities exists. Modern (and even near-future technology) will offer few options in the choice of irradiation or tracking systems or even in the construction of a vehicle itself. Thus, the choice of the right propellant is one of the few issues under control, and criteria are needed to compare the many materials available. A natural, and classical, figure of merit that can serve this purpose is the specific impulse.

Received 23 January 2001; revision received 24 September 2001; accepted for publication 26 October 2001.

*Assistant Professor, Department of Physics. Member AIAA.
†Professor, Department of Physics.
‡Graduate Student, Department of Physics. Student Member AIAA.

The specific impulse I_{sp} gained by a solid target exposed to a short laser pulse can be defined as

$$I_{sp} \equiv \frac{1}{W} \int_{t_0}^{t_f} F(t)\, dt \tag{1}$$

where W is the weight of the ablated propellant and $F(t)$ is the thrust as a function of time t. The integral presents an impulse applied to the target. For ALP the time interval (t_0, t_f) over which the integration takes place is defined by the duration of the ablation, which is of order of 1.0 μs (Ref. 6). Typically this interval is incomparably longer than the pulse width of the irradiating laser and is about equal to the plasma lifetime. The integration time interval distinguishes ALP from other LP techniques, for which the interval (t_0, t_f) is usually set equal to the laser pulse duration.[7] Applying Newton's second law to Eq. (1) will yield

$$I_{sp} = \frac{1}{W} \int_{t_0}^{t_f} \frac{dP(t)}{dt}\, dt = \frac{P}{W} = \frac{v}{g} \tag{2}$$

The last form of Eq. (2) gives I_{sp} in its well-known form: mean propellant velocity v divided by the acceleration caused by gravity ($g = 9.8$ m/s^2). P denotes the acquired momentum per pulse. Assuming that the mass cancelled out in Eq. (2) was ablated with the same mean velocity v, I_{sp} can be directly deduced from a measurement of the speed of the ablated ions.

As just stated, ALP must utilize high-energy short laser pulses. The question of "how short" can be addressed with the following simple argument. To make ablation the dominant mechanism of momentum transfer, the upper limit for the laser pulse duration must be set by the time needed for the development of high-density plasma, which becomes opaque for further transmission of laser energy. The total reflection of light by a plasma occurs when its complex refractive index becomes purely imaginary, which is equivalent to saying that the plasma frequency exceeds a critical value $\omega_{pc} = \omega$, the frequency of the incident light. The critical electron density N_{ec}, corresponding to ω_{pc}, can be derived from the following expression:

$$N_{ec} = \frac{m_e \varepsilon_0 \omega_{pc}^2}{e^2} \tag{3}$$

where m_e and e are electron mass and charge, respectively, and ε_0 denotes the permittivity of free space. Thus, for two major wavelengths of laser irradiation, 1.06 and 10.6 μm, the critical electron

density will be $\sim 3 \times 10^{25}$ and 3×10^{23} m^{-3}, respectively. Assuming that impact ionization is the dominant mechanism in electron density growth (i.e., neglecting multiphoton ionization) and that the timescales are short enough so that all major loss mechanisms can be neglected, the following simple equation results:

$$\frac{dN_e}{dt} = \nu N_e \tag{4}$$

where ν is the ionization rate. Integrating Eq. (4) and solving for t yields

$$t = \ell n(N_{ec})/\nu \tag{5}$$

Taking $\nu = 6 \times 10^{11}$ s^{-1} (Ref. 8) and substituting values of N_{ec} just calculated into Eq. (5), estimated critical times are t_c: 98 and 90 ps for 1.06- and 10.6-μm wavelengths, respectively. Thus, the upper limit for t_c is of the order of 100 ps, and it can actually be longer if two-photon absorption ($\nu = 5 \times 10^{10}$ s^{-1}, Ref. 8) and electron losses (caused primarily by attachment and recombination) are taken into account. Thus, effective ALP can be provided by energetic picosecond or shorter pulses, and only under such conditions can the technique be a reasonable alternative to other LP concepts. When momentum transfer is dominated by ablation, a strong dependence of I_{sp} on the particular propellant is expected. Therefore, a good choice for the appropriate propellant, providing high specific impulse, will be a key issue in the development of ALP. The purpose of this paper is to address this issue, primarily from an experimental point of view.

Experimental Technique

The experimental setup used in the present study is given in Fig. 1. This arrangement is essentially a time-of-flight (TOF) energy analyzer. The advantage of this architecture, compared to a direct force measuring system (also discussed later), is that it allows measurement of the angular distribution of the energy and the number density of the emitted ions (and with additional probes also the charge state of the ions). The TOF technique also does not require ex situ mass removal measurements to determine I_{sp}.

The laser system sketched in Fig. 1 is composed of a seeding laser (mode-locked Coherent Antares) and a regenerative amplifier (Continuum RGA60). The laser system was tuned to the second harmonic output (532-nm wavelength), and it was generating single or repetitively (up to 10 Hz) emitted pulses of width $\sim$100 ps and energy $\sim$35 mJ. Selection of the output pulse from the amplified train was monitored by a LeCroy 9450 Digital Storage Oscilloscope, whereas pulse energy was measured by a broadband energy/power meter (Melles-Griot 13PEM001). The light from the laser system (1) was focused onto the sample (2) through the optical window (3) by an external lens (4). Plano-convex lenses of focal length 20 and 50 cm were used as (4), providing irradiances at the diffraction limited spot on the target in the range $\sim 5 \times 10^{12}$–3×10^{13} W/cm^2. The optical window (3) was attached to the ablation chamber (5) at Brewster's angle to minimize reflection losses. The ablation chamber was maintained at vacuum $\sim 3 \times 10^{-3}$ torr by the pumping system (6), composed of roughing pump (Alcatel 2002 BB) and diffusion pump (Varian HS-2). The pressure was measured by a thermocouple gauge (Kurt Lesker KJL-6000), attached approximately 40 cm downstream from the sample. The pressure readings from the gauge were taken

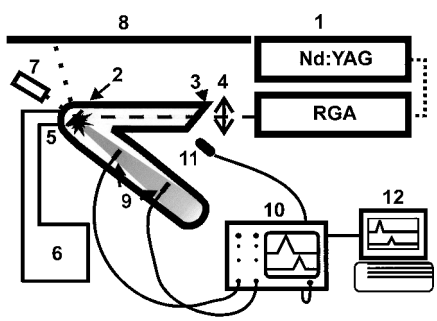

Fig. 1 Experimental setup.

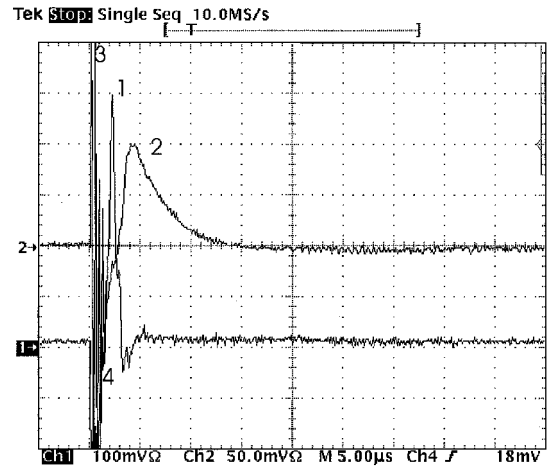

Fig. 2 TOF waveforms as seen on oscilloscope.

with the controller (Kurt Lesker IG4400), and this pressure provided the required mean free path of the ions (>0.2 m). The samples were attached to a holder, which allowed in vacuo translation and rotation along the vertical axis. Angles of rotation were measured with an accuracy $\sim$16 arcsec by means of a simple external optical reference system composed of a mirror attached to a sample holder, a positioning He-Ne laser (7) and a 6.7-m-long ruler (8) fixed along the laboratory wall.

The key measurements of ion velocity and yield were performed by the TOF energy analyzer (9). This system consisted of two copper plates separated by 20 cm and connected via a vacuum feed-through to a digital oscilloscope (10) (Tektronix TDS 460A). The oscilloscope was triggered by a photodiode (11) positioned near the optical window (3). The ion kinetic waveforms were recorded by the oscilloscope and then were analyzed on a personal computer (12) for velocities and number densities of ions using a set of programs written in Mathematica (Version 4.0).

The energy analyzer and oscilloscope allowed real-time recording of the waveforms corresponding to the charge deposited by ions striking the first and second plates successively. A typical pair of waveforms is presented in Fig. 2. The velocity of the ions can be found from the temporal separation of the peaks, denoted as 1 and 2 in Fig. 2. Ion yields were calculated from currents passing through the plates in assumption that the detected species are singly ionized. Maximum yields are achieved by rotation of the target until the normal to the target surface at the point of incidence is directed toward the corresponding plate of the detector. The sharp positive features at the beginning of the waveform (denoted in the figure as 3) are from photoelectrons emitted from the detector plates, whereas the negative peaks (4) are caused by deposition of electrons from the plasma.

A set of flat elemental targets representing a reasonably broad range of atomic masses was chosen: carbon (graphite), silicon (monocrystalline), aluminum, iron, copper, zinc, tin, gold, and lead. In addition, some compounds were examined, for example, the waveforms presented in Fig. 2 were obtained from a SiC sample.

Results and Discussion

Because every pulse from the laser removes a certain portion of matter from the target, it was important to record and use the data from shots that gave a steady-state signal. In Fig. 3 the I_{sp} deduced from a single-shot TOF measurement of a fixed lead target is presented as a function of the laser shot number. Three clearly distinct regions can be seen. A couple of the first shots gave suspiciously high values of I_{sp}, followed by a steady-state region, with a subsequent roll off of the signal after about 40 exposures. Region 1 can be attributed to surface contamination with low-Z elements, which give a higher I_{sp}. This low-Z and consequently high I_{sp} region can originate from the ablation of an oxide layer and/or a hydrocarbon contamination, which has been shown to be present in systems employing diffusion pumps.[9] In further analysis these first data points were discarded. Region 2 is the steady-state region, which

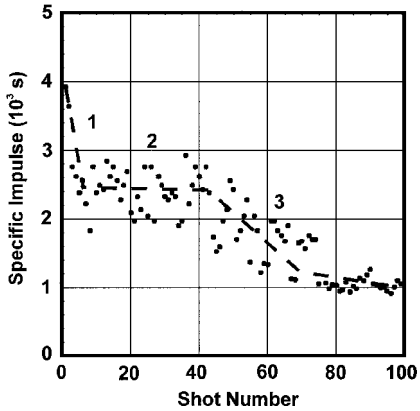

Fig. 3 Specific impulse vs laser shot number, as observed for an individual lead sample; – – –, trends in the data.

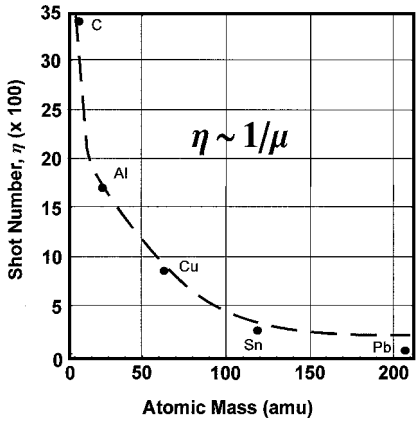

Fig. 4 Critical exposure η vs atomic mass; – – –, numerical fit (see text for details).

ends after about 40 shots (denoted later as a critical exposure number η). The 20% scatter observed in the data in region 2 is primarily caused by variation in the laser pulse power from shot to shot. When the critical exposure number of shots of the target was exceeded, a degradation of the waveforms from crater formation was observed (region 3 of Fig. 3). To ensure that data from region 2 were used exclusively, critical exposures for all targets used were determined. Observations indicated that the critical exposure decreased as the atomic mass of the sample increased, that is, high atomic mass gives low critical exposure. Thus, the extremes were represented by lead, where degradation of the signal was observed after only 40 shots, and graphite, where the signal was stable for more than ~3400 shots. These results are summarized in Fig. 4, where critical exposure is given as a function of atomic mass μ. A numerical fit clearly shows that η is inversely proportional to the atomic mass of the target. We will return to this result in the discussion of mass-removal rate data.

The major promise of ALP is the high specific impulse. The specific impulse as a function of atomic mass of the target is represented in Fig. 5. Each point representing an element on the graph was deduced from 3 to 5 distinct sets of measurements taken on different dates with seven measurements at different target spots per set. Separate measurements were taken using two focusing lenses with focal distances 20 and 50 mm. Though irradiance is assumed to decrease using lenses of increasing focal length, no significant reduction in I_{sp} was observed when the 50-mm lens was used in place of the 20 mm. The overall I_{sp} was marginally reduced, that is, if placed on Fig. 5, the curve for this higher focal length lens would shift downward but still be within the experimental error of the data from the 20-mm lens. A maximum specific impulse of about 2×10^4 s (corresponding to an ion velocity of 200 km/s) was obtained for carbon targets. The I_{sp} decreases proportionally to the inverse square root of the atomic mass of the element. Such behavior is characteristic of a Maxwellian velocity distribution, as it has been known since ruby lasers were first used in ablation studies.[10] However, the I_{sp}

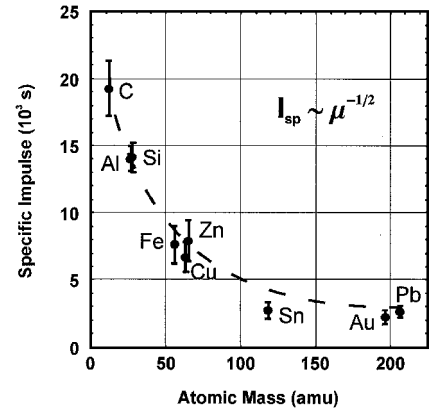

Fig. 5 Specific impulse vs atomic mass of propellant; – – –, numerical fit (see text for details).

values reported here exceed commonly expected limits for LP in general (~3×10^3 s, Ref. 11), as well as results reported previously for femtosecond irradiation,[3] and are overwhelmingly higher than the best known I_{sp} for conventional (chemical) propulsion (455 s, Ref. 12).

The anomalous behavior of lead ions reported in Refs. 3 and 13 was not observed in this work. Excluding experimental artifacts in Ref. 13, the behavior can be still attributed to the difference in irradiation conditions. An interesting feature was observed for compound targets, such as SiC. With the SiC targets placed at the focal spot, the TOF analyzer yielded velocities characteristic of pure Si targets. The same effect of dominant signals from heavier atoms was observed in early ablation experiments on mixed foils (Au + Ag), (Ag + Al), and (Ag + C) conducted by Fenner, who used similar experimental techniques.[14] These observations are worth additional study, which is now in progress. Returning to the major observation, it can be stated that the results presented in Fig. 5 basically set the direction for the development of candidate ALP propellants toward reasonably light elements. Carbon, silicon, aluminum, and perhaps combinations of these elements will likely constitute the best propellants providing the highest I_{sp} for ALP.

To reconstruct the overall picture of energy transfer from laser pulse to ejected ions, the angular distribution of ion energy and number density had to be determined. The angular dependence measurements were performed with the assumption that the angle of incidence of the laser pulse to the target would not significantly affect the energy deposited on the target. This assumption was reasonably supported by observation of the independence of I_{sp} on the angle of incidence in the ±70-deg range (Fig. 6a). The number of ions N collected per unit area of detector appeared to be proportional to the cosine of the polar angle θ (Fig. 6b). Thus N can be represented by a function:

$$N(\theta) = N_0 \cos\theta \tag{6}$$

where N_0 is the number of ions collected by a detector unit area at normal incidence to the target surface. In the time domain all of these quantities are integrated over the interval (t_0, t_f), as defined in Eq. (1). Keeping this in mind, further estimates in per-pulse terms can be made. The ion yield Y (that is, total number of ions emitted per laser pulse) can be estimated in spherical coordinates through a surface integration:

$$Y = \int_S N(\theta)\, \mathrm{d}a = \int_0^{2\pi} \int_0^{\pi/2} N_0 \cos\theta R^2 \sin\theta\, \mathrm{d}\theta\, \mathrm{d}\phi = \pi R^2 N_0 \tag{7}$$

where R is the distance from the focal spot on the target and ϕ is an azimuthal angle. (Rotational symmetry about ϕ is assumed.) Therefore, if the detector plate of area 1 cm^2 is placed at $R = 20$ cm away from the target (first plate) and detects 7×10^{10} ions per pulse, the total number of emitted ions per pulse can be estimated to be about 8.8×10^{13}.

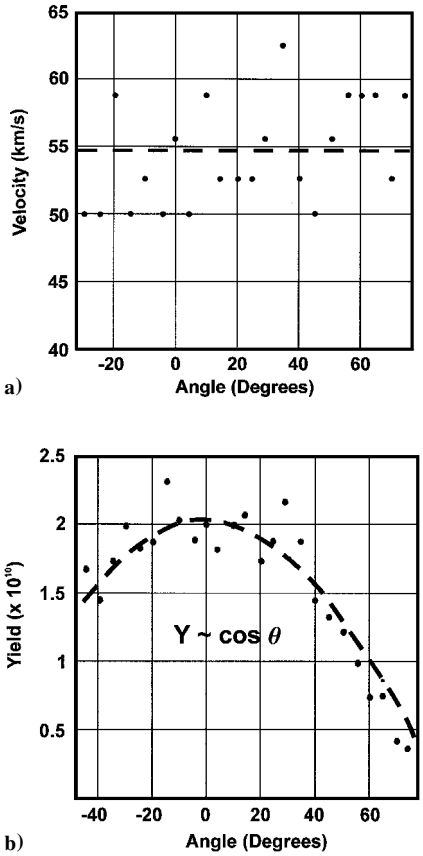

Fig. 6 Angular distributions of a) ion velocity and b) yield. These data were taken on copper samples; – – –, numerical fit (cosine for panel b).

From the data presented in Fig. 6, the net momentum vector $\boldsymbol{P}$, imparted to the target, can also be estimated. It is necessary to integrate vectors of momentum for all individual ions over the solid angle $\Omega = 2\pi$ sr (a hemisphere):

$$\boldsymbol{P} = \int_{\Omega} \mathrm{d}\boldsymbol{p} = \hat{n} \int_{\Omega} \hat{n} \cdot \mathrm{d}\boldsymbol{p} \tag{8}$$

The second integral in Eq. (8) reflects that only normal components of vectors will add to the integral and horizontal components will cancel out as a result of rotational symmetry ($\hat{n}$ denotes a unit vector normal to the target surface). Keeping in mind that the velocity distribution is angle independent (Fig. 6a), as $v(\theta) = v_0$, the scalar differential for momentum $\mathrm{d}p$ can be written as

$$\mathrm{d}p = \mathrm{d}(mv) = \mathrm{d}(mv_0) = v_0\,\mathrm{d}m = v_0\,\mathrm{d}(m_i N_\Omega \Omega) \tag{9}$$

where m_i is an ion mass and N_Ω is the number of ions emitted per pulse per steradian. Assuming that within an infinitesimal solid angle $\mathrm{d}\Omega$ the ion emission number N_Ω is constant, $\mathrm{d}(N_\Omega \Omega) = N_\Omega\,\mathrm{d}\Omega = N_\Omega \sin\theta\,\mathrm{d}\theta\,\mathrm{d}\phi$. Also, the relationship between N_Ω and N introduced here is merely $N_\Omega = R^2 N$. Therefore, $N_\Omega = N_{\Omega 0}\cos\theta$, where $N_{\Omega 0} = R^2 N_0$. Thus, the set of Eq. (9) can be rewritten as

$$\mathrm{d}p = v_0 m_i N_\Omega\,\mathrm{d}\Omega = v_0 m_i N_0 R^2 \cos\theta \sin\theta\,\mathrm{d}\theta\,\mathrm{d}\phi \tag{10}$$

This result can be substituted back into Eq. (8), from which the total ion momentum imparted on the target by a laser pulse can be found:

$$\boldsymbol{P} = \hat{n} \int_0^{2\pi} \int_0^{\pi/2} \cos\theta\, v_0 m_i N_0 R^2 \cos\theta \sin\theta\,\mathrm{d}\theta\,\mathrm{d}\varphi$$

$$= \frac{2}{3}\pi v_0 m_i R^2 N_0 \hat{n} = \frac{2}{3} v_0 m_i Y \hat{n} \tag{11}$$

(The first $\cos\theta$ in the integral originates from the dot product of $\hat{n}$ and $\mathrm{d}\boldsymbol{p}$.) The last result might seem counterintuitive: the total momentum is merely equal to two-thirds of the total number of emitted ions multiplied by momentum of an individual ion. However, this can be understood because the losses in total momentum (through the cancellation of the horizontal momentum components of individual ions) are compensated by a cosine "collimation" of the ion number density.

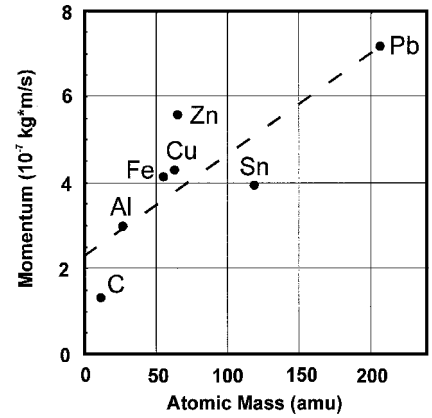

Fig. 7 Net momentum imparted to the target vs atomic mass of propellant; – – –, trend in the data.

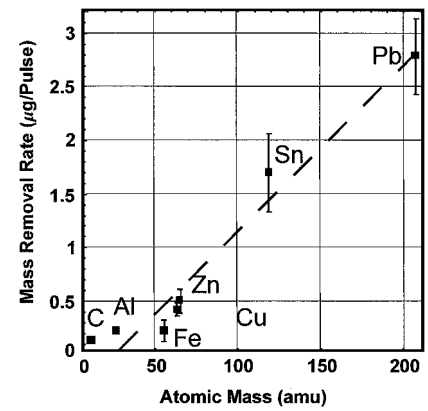

Fig. 8 Mass-removal rate vs atomic mass of propellant; – – –, trend in the data.

Figure 7 presents the momentum estimated from Eq. (11) as a function of atomic mass. Higher momentum is imparted to the targets by the heavier ions. This result is not really surprising, and it could be concluded from a much simpler estimation. Comparing two extreme elements of the current study, carbon and lead, one can anticipate that, whereas the carbon ions travel eight times faster (Fig. 5), they are still 17 times lighter than lead ions, and therefore the momentum will favor lead with a factor of two. Differences in ion yields will increase this gap by another ~2.7 factor, resulting in total factor of 5.4 difference. At this point, however, recall that ion yield estimates determined using Fig. 7 are based on the assumption of a singly ionized species. This assumption can be tested by determining ion states in the plasma using time-resolved emission spectroscopy, and such experiments are underway. However, there is a serious experimental evidence that allows us to expect that the content of multiply ionized species will be negligibly small.[15] Another way that allows a bypass of this issue is direct thrust measurement, which will be discussed next.

In the course of current experiments, mass-removal rates have also been measured by simply weighing the sample before and after exposure. Because of the minute amount of material ablated per shot, an accumulation of removed mass was achieved by using longer exposures, where the sample was periodically displaced to ensure that the number of shots was kept below the critical exposure η. Targets made of high-Z and therefore low η elements, such as lead, had to be moved several times to a new ablation spot in vacuo before the second weighing could be performed. Mass-removal rates for monocrystalline silicon wafers could not be determined because the samples usually cleaved before the needed exposure could be achieved. The results of mass-removal measurements are summarized in Fig. 8.

Table 1 Ion fraction and energy estimates

Parameter	Carbon	Aluminum	Iron	Copper	Zinc	Tin	Lead
Ion yield ($\times 10^{13}$)	5.3	7.3	9.1	9.3	9.9	11.6	12.3
Atoms ablated ($\times 10^{15}$)	6.5	4.9	2.4	4.0	4.6	8.6	8.1
Ion fraction, %	0.8	1.5	3.8	2.4	2.1	1.3	1.5
Ion energy, keV	2.21	2.63	1.59	1.40	2.03	0.42	0.70

Mass-removal rates are of order of μg/pulse and increase with atomic mass as shown in Fig. 8. These results are of the same order of magnitude as those reported by De Young and Situ, who used 8-ns, 400-mJ pulses generated by a Q-switched Nd:YAG laser.[16] The authors pointed out that observed mass-removal rates are $\sim$100 times lower than expected from simple evaporation (pulse energy divided by latent heat of vaporization). Similar mass-removal rates were achieved in the current study with a factor of 10 less pulse energy (35 mJ) and $\sim$100 times shorter pulses. This supports De Young and Situ's suggestion that in their case significant heat loss occurred via partial reflection of laser energy by a plasma.

The ion fraction for various elements estimated from mass-removal data is presented in Table 1. The estimations are made assuming single ionization and monoatomic removal (i.e., removal of larger fragments of the target is neglected). The ion yield presented in Table 1 was calculated according to Eq. (7). Ion fraction varies between 0.8% (carbon) and 3.8% (iron), and it closely matches previously reported ion fractions in Ref. 13 (see discussion in Ref. 13 and references therein). Of course, we should keep in mind that Table 1 presents ion fractions as they are observed 22 cm away from the target, while at much shorter distances and flight times (i.e., at the target surface) one must expect much higher ion content, close to 50% (Ref. 15). This fact raises the issue on justification for canceling mass in Eq. (2). In other words, the I_{sp} derived from Eq. (2) represents only ionic component of the ejecta. The fact that neutrals possessed less kinetic energy can also be seen from the data of Table 1. For example, assigning ion kinetic energy of 2.21 keV to each of the 6.5×10^{15} carbon atoms ablated per shot will yield an impossible total energy of 2.3 J, which exceeds the incident laser pulse energy by 100 times! In view of this result, the I_{sp} reported on Fig. 5 can be viewed as upper limit values, achievable only at ionization approaching 100% of all ablated material. Otherwise, these high I_{sp} values will be always dissolved by slower atomic neutrals and larger fragments.

To clarify the effect of neutrals on I_{sp} values, we have turned to direct measurements of temporal profiles of the thrust imparted on a target (in vacuo), from which total impulse transferred to the target can be deduced. The preliminary results of this study are reported in the Ref. 6. As expected, the I_{sp} values inferred from those measurements were 5–10 times less than ones presented in this study. Further clarification of this issue, as well as search for factors increasing I_{sp} such as optimal pulse separation, are currently in progress.

Data of Table 1 also provide a possible explanation as to why the critical exposure η appears inversely proportional to the atomic mass of the target (Fig. 4). This result can be understood if we assume that signal degradation is caused by crater formation. In our terms, η can be expressed through some characteristic critical mass of removed material m_c, which within the same experimental geometry must be a constant for all target materials. Then, critical mass and exposure will be related via the following equation:

$$\eta = \frac{m_c}{\rho V_{at} N_{at}} \tag{12}$$

where ρ is mass density of material, V_{at} is atomic volume, and N_{at} is the number of atoms removed per shot. As you can see from Table 1, with the possible exception of iron N_{at} does not vary too much from element to element. Atomic volume can be expressed as

$$V_{at} = \mu/\rho N_A \tag{13}$$

where N_A is Avogadro's number and μ represents the molar mass. Substituting Eq. (13) into Eq. (12) will yield

$$\eta = (m_c N_A/N_{at})(1/\mu) \tag{14}$$

where the first expression in the parentheses is approximately a constant. This result would imply that η times the mass-removal rate must yield the critical mass m_c. The data of Figs. 4 and 8 corroborate this result, giving the value of critical mass on the order of 0.4 mg with only 11% variation for all elements tested for η, with the exception of lead, which yielded 0.1 mg. This interesting result opens a new avenue for determining mass-removal rate from measurement of η (i.e., without actually using scales, or, say, with the least use of scales; m_c still must be measured once). Our experience shows that experimental assessment of η is a much more reliable measurement than determining miniscule mass differences after accumulating long exposures. This issue is currently under further study.

Returning to the issue of specific impulse, it can be stated that the trend in mass-removal rates supports low-Z elements as the best candidates for ALP. Thus, low-Z elements provide the highest specific impulse and, at the same time, suffer the lowest mass losses.

Therefore, successful ALP should be based on the ablation of low-Z solid elements such as carbon, aluminum, and the like. Alternatively, high-Z elements would provide higher thrusts. Keeping these dependences in mind, perhaps some "tuning" of specific impulse and thrust could be attained by layering different ablative materials so that the acceleration of the vehicle could be controlled without the effort of controlling the laser source itself.

Conclusions

Experimental evidence supporting a recently revived concept of ablative laser propulsion is presented. Upper limits for specific impulse from elementary targets ablated at irradiances of $\sim 3 \times 10^{13}$ W/cm^2 by 10^{-10} s width laser pulses are set at levels of 2×10^4 s for carbon and, in general, are inversely proportional to the square root of the atomic mass of the ablative. It was also observed that lighter elements produce much lower mass-removal rates, whereas heavier elements provide higher thrusts. In general, the results of this work leads to the conclusion that efficient ablative laser propulsion, providing the highest specific impulse, must be based on solid, low-Z propellants such as carbon or aluminum.

Acknowledgments

The partial support of this work by NASA STTR Phase I Contract NAS8-00185 and Information Systems Labs., Inc., NSF REU Grant ATM9820339 and UAH Mini-Grant Research Program is greatly appreciated. The authors would like to acknowledge support of their work by other physics faculty members, in particular by Lloyd W. Hillman, Matthew H. Smith, and Fred Seeley. The authors also appreciate all discussions and technical help provided by former and current student members of the Laser Propulsion Group, especially by Wesley Swift Jr. and Eric Broyles.

References

[1]Kantrowitz, A., "Propulsion to Orbit by Ground Based Lasers," *Aeronautics and Astronautics,* Vol. 9, No. 3, 1972, pp. 40–42.

[2]Mead, F. B., Jr., Myrabo, L. N., and Messitt, D. G., "Flight Experiments and Evolutionary Development of a Laser Propelled, Trans-Atmospheric Vehicle," *SPIE Conference on High-Power Laser Ablation*, Vol. 3343, Pt. 2, edited by C. Phipps, Society of Photo-Optical Instrumentation Engineers (International Society for Optical Engineering), Santa Fe, NM, 1998, pp. 560–563.

[3]Pakhomov, A. V., and Gregory, D. A., "Ablative Laser Propulsion: An Old Concept Revisited," *AIAA Journal*, Vol. 38, No. 4, 2000, pp. 725–727.

[4]Glumb, R. J., and Krier, H., "Concepts and Status of Laser-Supported Rocket Propulsion," *Journal of Spacecraft and Rockets*, Vol. 21, No. 1, 1984, 70–79.

[5]Caveny, L. H. (ed.), *Orbit-Raising and Maneuvering Propulsion: Research Status and Needs*, Vol. 89, Progress in Astronautics and Aeronautics, AIAA, New York, 1984, pp. 1–200.

[6]Pakhomov, A. V., Thompson, M. S., Gregory, D. A., and Swift, W., Jr., "Specific Impulse Study of Ablative Laser Propulsion," AIAA Paper 2001-3663, July 2001.

[7]Pirri, A. N., Monsler, M. J., and Nebolsine, P. E., "Propulsion by Absorption of Laser Radiation," *AIAA Journal*, Vol. 12, No. 9, 1974, pp. 1254–1261.

[8]Weyl, G. M., "Physics of Laser-Induced Breakdown: An Update," *Laser-Induced Plasmas and Applications,* edited by L. J. Radziemski and D. A. Cremers, Marcel Dekker, New York, 1989, pp. 1–67.

[9]Gitomer, S. J., Jones, R. D., Begay, F., Ehler, A. W., Kephart, J. F., and Kristal, R., "Fast Ions and Hot Electrons in the Laser-Plasma Interaction," *Physics of Fluids*, Vol. 29, No. 8, 1986, pp. 2679–2688.

[10]Linlor, W. I., "Energetic Ions Produced by Laser Pulse," *Laser Interaction and Related Plasma Phenomena,* edited by H. J. Schwartz and H. Hora, Plenum, New York, 1971, pp. 173–206.

[11]Schmidt, G., "MSFC Propulsion Research," *Proceedings of NASA/JPL/MSFC/AIAA Annual 10th Advanced Space Propulsion Workshop*, Vol. 1, edited by C. Barret and S. Leifer, Univ. of Alabama, Huntsville, AL, 1999, pp. 45–61.

[12]Wilson, A. (ed.), *Jane's Space Directory 1993-94*, Jane's Information Group, Ltd., Coulsdon, Surrey, England, U.K., 1993, p. 303.

[13]Pakhomov, A. V., Roybal, A. J., and Duran, M. S., "Ion Dynamics of Plasmas Induced in Elemental Targets by Femtosecond Laser Irradiation," *Applied Spectroscopy*, Vol. 53, No. 8, 1999, pp. 979–986.

[14]Fenner, N. C., "Ion Energies in the Plasma Produced by a High Power Laser," *Physics Letters*, Vol. 22, No. 4, 1966, pp. 421, 422.

[15]Fajardo, M. E., "Velocity Selection of Fast Laser Ablated Metal Atoms by a Novel Nonmechanical Technique: Temporally and Spatially Specific Photoionization (TASSPI)," U.S. Air Force Research Lab./PRS, Final Rept. PL-TR-97-3051, Edwards AFB, CA, Feb. 1998.

[16]De Young, R. J., and Situ, W., "Elemental Mass-Spectroscopy of Remote Surfaces from Laser-Induced Plasmas," *Applied Spectroscopy*, Vol. 48, No. 11, 1994, pp. 1297–1306.

M. Sichel
Associate Editor